LETTERS

Crystal structure of the sodium–potassium pump at 2.4 Å resolution

Takehiro Shinoda[1], Haruo Ogawa[1], Flemming Cornelius[2] & Chikashi Toyoshima[1]

Sodium–potassium ATPase is an ATP-powered ion pump that establishes concentration gradients for Na^+ and K^+ ions across the plasma membrane in all animal cells by pumping Na^+ from the cytoplasm and K^+ from the extracellular medium[1,2]. Such gradients are used in many essential processes, notably for generating action potentials. Na^+,K^+-ATPase is a member of the P-type ATPases, which include sarcoplasmic reticulum Ca^{2+}-ATPase and gastric H^+,K^+-ATPase, among others, and is the target of cardiac glycosides. Here we describe a crystal structure of this important ion pump, from shark rectal glands, consisting of α- and β-subunits and a regulatory FXYD protein[3,4], all of which are highly homologous to human ones. The ATPase was fixed in a state analogous to $E2{\cdot}2K^+{\cdot}P_i$, in which the ATPase has a high affinity for K^+ and still binds P_i, as in the first crystal structure of pig kidney enzyme at 3.5 Å resolution[5]. Clearly visualized now at 2.4 Å resolution are coordination of K^+ and associated water molecules in the transmembrane binding sites and a phosphate analogue (MgF_4^{2-}) in the phosphorylation site. The crystal structure shows that the β-subunit has a critical role in K^+ binding (although its involvement has previously been suggested[6–8]) and explains, at least partially, why the homologous Ca^{2+}-ATPase counter-transports H^+ rather than K^+, despite the coordinating residues being almost identical.

The structure was determined using heavy-atom derivatives (Supplementary Table 1). Bound K^+ could be substituted by dialysis for Tl^+ and Rb^+, whose anomalous electron density maps showed three binding sites (two transmembrane (I and II) and one cytoplasmic (C); Figs 1b and 2d). The K^+ at site C is implicated in activation of dephosphorylation[9]. The atomic model (Fig. 1) was refined to an R_{free} value of 27.6% at 2.4 Å resolution (Supplementary Table 1) and for the α-subunit was, in general, very similar to that for pig kidney ATPase at 3.5 Å resolution[5]. The extracellular parts of the β-subunit and the FXYD protein have not been modelled previously.

Detailed comparison of the structure with the Ca^{2+}-ATPase in the corresponding state ($E2{\cdot}nH^+{\cdot}P_i$; Supplementary Fig. 1)[10] revealed important differences pertinent to those in function, although each of the three cytoplasmic domains[11] and transmembrane helices (M1–M10) are superimposable (Fig. 2). In Ca^{2+}-ATPase, the cytoplasmic headpiece has a compact configuration[10], stabilized, in part, by two hydrogen bonds between the actuator (A) and nucleotide (N) domains (Fig. 2d). In Na^+,K^+-ATPase, the A and N domains hardly interact, with only one salt bridge involving Glu 223 (A; corresponding to Val 185 in Ca^{2+}-ATPase) and Arg 551 (N; Arg 560) between them (Figs 1 and 2d). The N domain of Na^+,K^+-ATPase is ~22° further from the P domain than that of Ca^{2+}-ATPase (Fig. 2a), which is perhaps pertinent to the much faster ATPase turnover (~200 s^{-1} versus ~30 s^{-1}).

As the ATP-binding site is located just above this salt bridge, the ATP molecule in $E2{\cdot}ATP(TG)$ of Ca^{2+}-ATPase can be docked at the equivalent position (Fig. 2d). With ATP here, Arg 551 is likely to form a salt bridge to the β-phosphate. In fact, the Arg551→Gln mutation abolishes ATP binding[12]. Arg 560, the corresponding residue in Ca^{2+}-ATPase, interacts with the β-phosphate[13,14] and is a key residue in ATP binding[15]. As both ADP and ATP hinder formation of the complex with MgF_4^{2-} (ref. 16), it is likely that nucleotides disrupt the Glu 223–Arg 551 salt bridge, aiding dissociation of the A and N domains. If this salt bridge were maintained in $E2{\cdot}2K^+$, the well-known accelerating effect of ADP and ATP on K^+ release[2] would be readily explained. Such acceleration effects of ATP, though to a lesser degree, are also known for Ca^{2+}-ATPase (see, for example, ref. 17), and Arg 489 (N) appears to play a similar role together with Asp 203 (A)[18].

In the transmembrane region, the unwinding of M5 (at Asn 783) and M7 (at Gly 855) in Na^+,K^+-ATPase stands out (Fig. 1c). The segment of M7 near the cytoplasmic surface (M7′) has a distinct kink of ~18° (Fig. 2a), which appears to have central importance in K^+ binding. At 2.4 Å resolution, the coordination geometry of K^+ and associated water molecules is evident. Site I is made essentially of only five oxygen atoms, contributed by one main chain (Thr 779), three side chains (Ser 782, Asn 783 and Asp 811) and one water molecule (Fig. 3). The closest oxygen atom of Glu 786 (Glu 771 in Ca^{2+}-ATPase) is 3.9 Å away and does not contribute. Site I has a valence[19] of 1.06 (Supplementary Table 2), and is well qualified to be a high-affinity K^+ site (ideal valence, 1.0).

The site-II K^+ is shifted by 1.3 Å to the extracellular side in comparison with the site-I K^+ (Fig. 3b). It is coordinated by three main-chain carbonyls (Val 329, Ala 330 and Val 332), three or four side-chain oxygen atoms (Asn 783, Glu 786, Asp 811 and possibly Glu 334) and no water molecules (Fig. 3). Although the coordination number is high (six or seven), the sum of partial valences is lower than for site I, being 0.64 (Supplementary Table 2). Glu 334 on M4 (equivalent to Glu 309 in Ca^{2+}-ATPase) is structurally a very important residue, consistent with mutagenesis results[20–22], but marginally qualifies as a K^+-binding residue with the carboxyl 3.3 Å away (partial valence, 0.03). Thus, the two K^+ sites have different coordination characteristics but coordination geometry is rather distorted at both sites. The sum of partial valences[19] calculated for Na^+ is 0.62 at site I and 0.54 at site II (Supplementary Table 2), explaining the lower affinity for Na^+ in this state.

Unexpectedly, Asp 815, which is equivalent to Asp 800 in Ca^{2+}-ATPase and therefore expected to play a pivotal role in Na^+ binding[23], does not coordinate K^+, although it fixes a coordinating water at site I (Fig. 3). Gln 930 on M8 (equivalent to Glu 908 in Ca^{2+}-ATPase) is far from the bound K^+, but appears to stabilize the Asp 815 side chain, which is also stabilized by the Tyr 778 hydroxyl. Thus, they might contribute to adjust the affinity for K^+.

A possibly more unexpected observation is that the two bound K^+ ions (ionic radius, 1.35 Å) are juxtaposed only 4.1 Å apart, with no

[1]Institute of Molecular and Cellular Biosciences, The University of Tokyo, Bunkyo-ku, Tokyo 113-0032, Japan. [2]Department of Physiology and Biophysics, University of Aarhus, DK-8000 Aarhus C, Denmark.

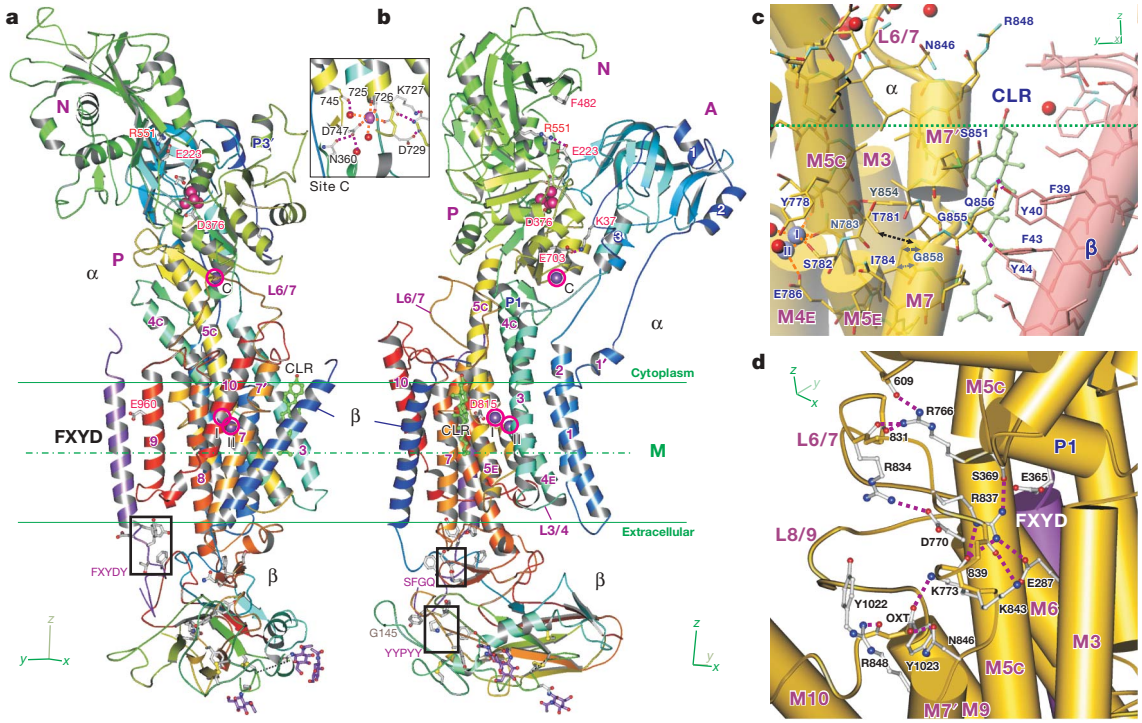

Figure 1 | Architecture of Na^+,K^+-ATPase with bound MgF_4^{2-} and K^+. **a**, **b**, Ribbon diagrams. **c**, **d**, Details around the unwound part of M7 (**c**) and the L6/7 loop (**d**). In **a** and **b**, the colour changes gradually between the amino-terminal (blue) and carboxy-terminal (red) ends for the α- and β-subunits. The FXYD protein is in purple. Circled purple spheres represent bound K^+ ions. A cholesterol molecule (CLR), sugars and several key residues are depicted in ball-and-stick style. The *x* and *y* axes respectively correspond to the *a* and *b* axes of the crystals. The membrane plane appears to lie at an inclination of ~4° from the *a*–*b* plane (Supplementary Fig. 2b). Inset, detail at the K^+-binding site in the phosphorylation (P) domain (site C); the coordination geometry is largely different from that in the pig kidney model[9]. The horizontal green lines show the approximate boundaries of the hydrophobic core of the lipid bilayer. Common motifs in the extracellular region are boxed. Hydrogen bonds (broken purple lines), K^+ coordination (broken orange lines) and van der Waals contacts (broken black arrows) are also shown. The dotted line in the β-subunit shows the part (nine residues) for which the atomic model was not built (**a**). The amino-terminal 31 residues of the α-subunit and 27 residues of the β-subunit and the carboxy-terminal 33 residues of FXYD10, all in the cytoplasm, could not be modelled. M, membrane; P1, P3′, α-helices in the P domain; OXT, terminal carboxyl oxygen.

intervening oxygen atom. Two side-chain oxygen atoms of Asp 811 and Asn 783 are shared by the two K^+ ions, but there is no carboxyl group bridging them. This is in marked contrast with the Ca^{2+}-binding sites in Ca^{2+}-ATPase[11], in which Asp 800 bridges the two Ca^{2+} ions, and no oxygen atom is shared by them. The short distance between the two K^+ ions and the orientation of Asp 811 are related to the binding cavity being highly confined.

Homology modelling based on Ca^{2+}-ATPase crystal structures[23] correctly predicted many features of the K^+-binding sites, indicating the similarity of these two pumps. For instance, according to the predictions a larger binding cavity for K^+ is created by bowing of M5 towards M1, which removes Glu 786 from site I and brings in the smaller Ser 782 instead, and rotation of M6 brings in Asp 811 and removes Thr 814 from site I. However, perhaps the most striking observation is that the positions of the coordinating residues, and even the conformations of the side chains, are virtually identical, except for that of Asn 783 (Fig. 3). Yet, whereas the K^+-binding sites in Na^+,K^+-ATPase accommodate other monovalent alkali cations including Na^+ and H^+ (see, for example, ref. 1), Ca^{2+}-ATPase binds only H^+ for counter-transport[24].

The crystal structures explain this. It is noteworthy that the K^+-binding sites are fairly confined and offset in comparison with the Ca^{2+} sites, very close to the M4 and M5 helices (Fig. 3a), despite K^+ being substantially larger than Ca^{2+} (1.35 Å versus 0.99 Å). This is a natural consequence of employing a main-chain carbonyl for coordinating K^+ at site I, rather than, for instance, the Asp 815 carboxyl as predicted[23]. In fact, usage of a main-chain carbonyl appears to be the key in defining ion selectivity.

A marked difference from Ca^{2+}-ATPase is the presence of Pro 785 on the M5 helix of Na^+,K^+-ATPase (instead of Gly 770 in Ca^{2+}-ATPase). Because of this Pro, M5 of Na^+,K^+-ATPase is unwound and kinked (~18°) such that the main-chain oxygen of Thr 779 becomes available for K^+ coordination (Fig. 3b). M5 of Ca^{2+}-ATPase is similarly kinked (Figs 2a and 3b), but is a continuous helix, creating little extra space. Reflecting this, the main-chain positions of Asn 783 and the corresponding Asn 768 are critically different. The amide of Asn 768 in Ca^{2+}-ATPase comes too close to the site-I K^+ (3.0 Å versus 3.8 Å; Fig. 3b), and the side chain too close to the site-II K^+, to allow K^+ binding. In Na^+,K^+-ATPase, the side chain of Asn 783, the corresponding residue, has a distinct conformation fixed by a hydrogen bond with Tyr 854, made possible by the kink of M7′ (Figs 2c and 3a). The cytoplasmic end of M7′ is positioned by a rigid L6/7 loop, critically linked to M3 and M5 with hydrogen bonds involving Arg 766 and Arg 837 (Fig. 1d), known as loci of familial hemiplegic migraine[25], and Glu287, a locus of rapid-onset dystonia-parkinsonism[26].

In Ca^{2+}-ATPase, the M5 helix straightens[18] during the $E2P \rightarrow E2 \rightarrow E1{\cdot}2Ca^{2+}$ transitions. If a similar movement takes place in Na^+,K^+-ATPase, straightening of M5 will push M7′ towards M10 (Fig. 2e), which in turn will cause large-scale structural changes involving P1, M3 and the carboxy-terminal segment of the α-subunit as well as the β-subunit, owing to the extensive hydrogen-bonding network (Fig. 1d). Thus, helices M7–M10, which looked like a mere membrane anchor in Ca^{2+}-ATPase, appear to have a dynamic role in Na^+,K^+-ATPase and might be used to change the position of the cytoplasmic domain of the β-subunit. We expect that the Asn 783 side chain will change its position to interact with the smaller Na^+ with the help of Pro 785, as the interactions between M5 and M7′, including hydrogen bonding between Asn 783 and Tyr 854, will break.

Thus, unwinding of M7 appears to be of central importance in K^+ binding. This unwinding is stabilized by hydrogen bonding of Tyr 44

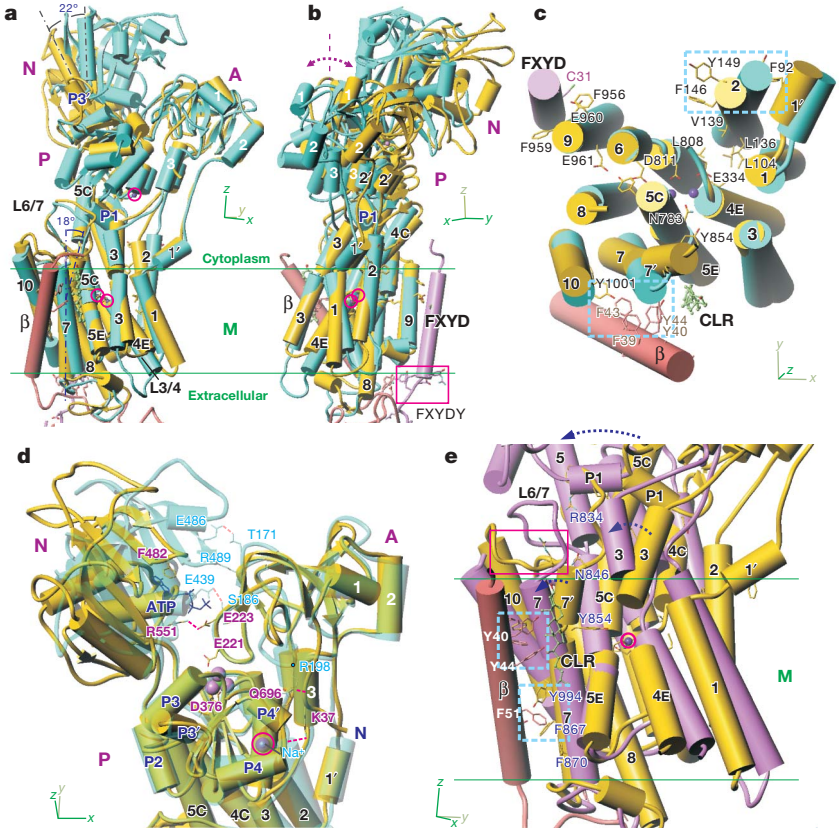

Figure 2 | Superimposition of the crystal structure of Na^+,K^+-ATPase on that of Ca^{2+}-ATPase. The structures are aligned with the six metal-coordinating residues[11] (**a**–**c**, **e**) or the P domain (**d**). In **a**–**d**, the E2·MgF_4^{2-}(TG) form of Ca^{2+}-ATPase (Protein Data Bank accession number, 1WPG) is superimposed; in **e**, the E1·$2Ca^{2+}$ form. The α-subunit of Na^+,K^+-ATPase is always in yellow, and the β-subunit in brown; the E2·MgF_4^{2-}(TG) form of Ca^{2+}-ATPase is in lime, the E1·$2Ca^{2+}$ form in violet. Although M3 is a continuous helix in both ATPases, it is represented by two cylinders. M5 and M7 are continuous helices in Ca^{2+}-ATPase but contain an unwound part in Na^+,K^+-ATPase; they are represented by three and two cylinders, respectively. In **e**, the transmembrane part of M3 is removed. Bound K^+ ions are represented by purple spheres in **a**–**c** and **e** (and marked with red circles). In **d**, MgF_4^{2-} and K^+ at site C (together with the corresponding Na^+ (cyan) in Ca^{2+}-ATPase) are shown in space-fill style, and cholesterol (CLR) in ball-and-stick style; an ATP taken from the E2·ATP(TG) form of Ca^{2+}-ATPase (Protein Data Bank accession number, 2DQS) is depicted using black sticks. The arrows in **e** indicate the expected movements in transition to the E1·$3Na^+$ state. The FXYDY motif (red box in **b**), the carboxy-terminal 10 residues (red box in **e**), and clusters of aromatic residues (cyan boxes in **c** and **e**) are also shown. TG, thapsigargin.

of the β-subunit to the Gly 855 carbonyl (Fig. 1c), which otherwise would be exposed to the hydrophobic core of the bilayer. Therefore, Ca^{2+}-ATPase cannot bind K^+ partly because it does not have a β-subunit. We note that there is a cholesterol molecule here (Fig. 1c and Supplementary Fig. 3), which appears to shield the unwound part of M7 from the bulk lipid. Its presence here is potentially related to a strong dependence of the Na^+,K^+-ATPase activity on cholesterol[27,28]. This cholesterol molecule, carried through from the native tissue, occupies the position in which a phospholipid head group was previously located[5].

The β-subunit is a single spanning membrane protein important in targeting and stabilization, but also affects the ion-binding and transport properties[8]. Its extracellular domain is large and rich in aromatic residues (Supplementary Fig. 4) and is glycosylated. We identified sugar residues at two of four potential sites (Fig. 1). The transmembrane helix of the β-subunit runs rather detached from those of the α-subunit and is inclined by ~32° from the membrane normal, nearly parallel to αM7 (Fig. 2). However, it forms four hydrogen bonds and numerous contacts with two transmembrane helices of the α-subunit, primarily using two clusters of aromatic residues. The first cluster, at about the level of the cholesterol ring, is formed from four residues (Phe 39–Tyr 44) of the β-subunit and one (Tyr 1001) from M10 of the α-subunit (Fig. 2c). Both Tyr 40 and

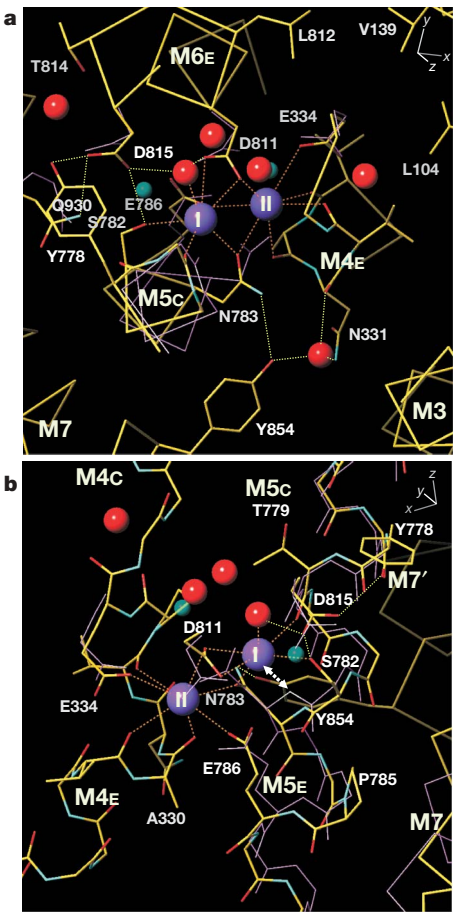

Figure 3 | Transmembrane K^+-binding sites. **a**, View from the cytoplasmic side; **b**, view approximately parallel to the membrane. Main chains of the M5 and M7 helices and side chains of the Ca^{2+}-coordinating residues of Ca^{2+}-ATPase (violet lines) are superimposed. The two structures are aligned with the metal-coordinating residues. Purple spheres represent bound K^+ ions, and red spheres water molecules; small cyan spheres (transparent) show the positions of bound Ca^{2+} ions in the E1·$2Ca^{2+}$ state of Ca^{2+}-ATPase. K^+ coordination (broken orange lines), hydrogen bonds (broken green lines) and a steric clash expected between K^+ at site I and the Asn 768 amide in Ca^{2+}-ATPase (corresponding to Asn 783 in Na^+,K^+-ATPase; white arrows in **b**) are also depicted. A stereo version of this figure is presented as Supplementary Fig. 6.

Tyr 44 interact with αM7 and cholesterol (Fig. 1c). They are highly conserved and the mutagenesis changes the apparent K^+ affinity[7]. The other cluster is in the extracellular leaflet of the bilayer, to which seven aromatic residues on four helices participate (Fig. 2e).

On the extracellular side, the carboxy-terminal part of the L7/8 loop (Asp 892–Gln 910) is the primary interaction site, in which a consensus sequence ^{901}SFGQ, proposed as a key interaction site[29], is located (Figs 1 and 4). The well-conserved Tyr 247 in the ^{244}YYPYY motif of the β-subunit fixes βArg 183 to mediate a salt bridge with αGlu 899, which in turn forms a salt bridge with βLys 250 (Fig. 4). Such complex interactions between the β- and α-subunits should explain, at least partly, previous results that implicate the β-subunit in modulation of cation transport[6,8].

Na^+, K^+-ATPase from shark rectal glands contains an accessory regulatory protein, FXYD10[3]. The transmembrane part runs approximately perpendicular to the membrane (Fig. 1a), interacting almost exclusively with the outside of αM9. Two conserved Gly residues, in particular Gly 34, are evidently important for this (Supplementary Fig. 5). Likely hydrogen bonds are found only between Cys 31 and αGlu 960. As the αGlu 960 carboxyl will be exposed to the hydrophobic part of the membrane if FXYD is absent (Fig. 2c), it will have to find a hydrogen-bond partner inside the α-subunit. Hence, it is conceivable that FXYD10 plays an important regulatory role through interactions with αGlu 960.

The role of the signature motif FXYD appears clear (Fig. 4). The first residue, Phe 12, anchors the segment to the β-subunit and the last residue, Asp 15, caps the helix. The third residue, Tyr 14, and the subsequent Tyr 16 form a cluster of aromatic residues with βTyr 69 and αTrp 987 to sandwich the β-subunit, together with the α-subunit. Glu 10/Arg 11 and Tyr 16 mediate a complex hydrogen-bonding network involving both subunits. Thus, functionally the motif should be considered to be FXYDY/W. The last Tyr is substituted for Trp in FXYD3 and FXYD4, but its indole ring will function similarly as the hydrogen donor to βAsp 71.

Previous studies located FXYD in the groove surrounded by M2, M6 and M9, following the model proposed for phospholamban[30], a regulatory protein for Ca^{2+}-ATPase that alters Ca^{2+} affinity presumably by interfering with the movement of M2. Three residues on M2 and another on M1 form an aromatic cluster there (Fig. 2c), apparently preventing access of a transmembrane helix.

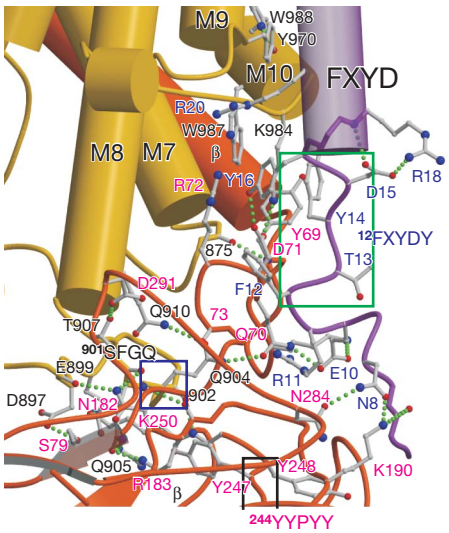

Figure 4 | Interactions among the α- and β- subunits and the FXYD protein at the extracellular surface of the membrane. View approximately parallel to the membrane. Conserved motifs are identified with boxes. Dotted lines represent hydrogen bonds. Four regions of the β-subunit contribute to interactions with the α-subunit: Tyr 69–Tyr 83 (also interacting with FXYD), Asn 182–Ile 185, Tyr 247–Lys 250 and Lys 290–Asp 291. Key residues appear to be Glu 899, Gln 904 and Gln 905 on the α-subunit and Asn 182 and Arg 183 on the β-subunit. Gln 905 is a locus of familial hemiplegic migraine[25]. A stereo version of this figure is presented as Supplementary Fig. 7.

METHODS SUMMARY

Na^+, K^+-ATPase was isolated from shark rectal glands and purified by mild deoxycholate extraction followed by differential centrifugation. This preparation contained the α- and β-subunits and an equimolar amount of FXYD10 (ref. 3). Crystals were grown by the dialysis method, supplemented with phosphatidylcholine, in the presence of MgF_4^{2-} and K^+ or its congener. Molecular replacement starting from the published model[5] was successful for resolving the α-subunit and FXYD. Multiple isomorphous replacement was performed to model the β-subunit.

Full Methods and any associated references are available in the online version of the paper at www.nature.com/nature.

Received 30 July 2008; accepted 26 February 2009.

1. Albers, R. W. Biochemical aspects of active transport. *Annu. Rev. Biochem.* **36,** 727–756 (1967).
2. Post, R. L., Hegyvary, C. & Kume, S. Activation by adenosine triphosphate in the phosphorylation kinetics of sodium and potassium ion transport adenosine triphosphatase. *J. Biol. Chem.* **247,** 6530–6540 (1972).
3. Mahmmoud, Y. A., Vorum, H. & Cornelius, F. Identification of a phospholemman-like protein from shark rectal glands. Evidence for indirect regulation of Na,K-ATPase by protein kinase c via a novel member of the FXYDY family. *J. Biol. Chem.* **275,** 35969–35977 (2000).
4. Garty, H. & Karlish, S. J. Role of FXYD proteins in ion transport. *Annu. Rev. Physiol.* **68,** 431–459 (2006).
5. Morth, J. P. *et al.* Crystal structure of the sodium–potassium pump. *Nature* **450,** 1043–1049 (2007).
6. Lutsenko, S. & Kaplan, J. H. An essential role for the extracellular domain of the Na,K-ATPase β-subunit in cation occlusion. *Biochemistry* **32,** 6737–6743 (1993).
7. Hasler, U., Crambert, G., Horisberger, J. D. & Geering, K. Structural and functional features of the transmembrane domain of the Na,K-ATPase β subunit revealed by tryptophan scanning. *J. Biol. Chem.* **276,** 16356–16364 (2001).
8. Geering, K. The functional role of β subunits in oligomeric P-type ATPases. *J. Bioenerg. Biomembr.* **33,** 425–438 (2001).
9. Schack, V. R. *et al.* Identification and function of a cytoplasmic K^+ site of the Na^+, K^+ -ATPase. *J. Biol. Chem.* **283,** 27982–27990 (2008).
10. Toyoshima, C., Nomura, H. & Tsuda, T. Lumenal gating mechanism revealed in calcium pump crystal structures with phosphate analogues. *Nature* **432,** 361–368 (2004).
11. Toyoshima, C., Nakasako, M., Nomura, H. & Ogawa, H. Crystal structure of the calcium pump of sarcoplasmic reticulum at 2.6 Å resolution. *Nature* **405,** 647–655 (2000).
12. Jacobsen, M. D., Pedersen, P. A. & Jorgensen, P. L. Importance of Na,K-ATPase residue alpha 1-Arg544 in the segment Arg544-Asp567 for high-affinity binding of ATP, ADP, or MgATP. *Biochemistry* **41,** 1451–1456 (2002).
13. Toyoshima, C. & Mizutani, T. Crystal structure of the calcium pump with a bound ATP analogue. *Nature* **430,** 529–535 (2004).
14. Sørensen, T. L., Møller, J. V. & Nissen, P. Phosphoryl transfer and calcium ion occlusion in the calcium pump. *Science* **304,** 1672–1675 (2004).
15. Clausen, J. D., McIntosh, D. B., Vilsen, B., Woolley, D. G. & Andersen, J. P. Importance of conserved N-domain residues Thr441, Glu442, Lys515, Arg560, and Leu562 of sarcoplasmic reticulum Ca^{2+}-ATPase for MgATP binding and subsequent catalytic steps. Plasticity of the nucleotide-binding site. *J. Biol. Chem.* **278,** 20245–20258 (2003).
16. Murphy, A. J. & Hoover, J. C. Inhibition of the Na,K-ATPase by fluoride. Parallels with its inhibition of the sarcoplasmic reticulum CaATPase. *J. Biol. Chem.* **267,** 16995–17000 (1992).
17. Jensen, A. M., Sørensen, T. L., Olesen, C., Møller, J. V. & Nissen, P. Modulatory and catalytic modes of ATP binding by the calcium pump. *EMBO J.* **25,** 2305–2314 (2006).
18. Toyoshima, C. & Nomura, H. Structural changes in the calcium pump accompanying the dissociation of calcium. *Nature* **418,** 605–611 (2002).
19. Brown, I. D. & Wu, K. K. Empirical parameters for calculating cation-oxygen bond valences. *Acta Crystallogr. B* **32,** 1957–1959 (1976).
20. Jewell-Motz, E. A. & Lingrel, J. B. Site-directed mutagenesis of the Na,K-ATPase: consequences of substitutions of negatively-charged amino acids localized in the transmembrane domains. *Biochemistry* **32,** 13523–13530 (1993).
21. Nielsen, J. M., Pedersen, P. A., Karlish, S. J. & Jorgensen, P. L. Importance of intramembrane carboxylic acids for occlusion of K^+ ions at equilibrium in renal Na,K-ATPase. *Biochemistry* **37,** 1961–1968 (1998).
22. Vilsen, B. & Andersen, J. P. Mutation to the glutamate in the fourth membrane segment of Na^+,K^+-ATPase and Ca^{2+}-ATPase affects cation binding from both sides of the membrane and destabilizes the occluded enzyme forms. *Biochemistry* **37,** 10961–10971 (1998).

23. Ogawa, H. & Toyoshima, C. Homology modeling of the cation binding sites of Na^+K^+-ATPase. *Proc. Natl Acad. Sci. USA* **99,** 15977–15982 (2002).
24. Ueno, T. & Sekine, T. Study on calcium transport by sarcoplasmic reticulum vesicles using fluorescence probes. *J. Biochem.* **84,** 787–794 (1978).
25. Pietrobon, D. Familial hemiplegic migraine. *Neurotherapeutics* **4,** 274–284 (2007).
26. de Carvalho Aguiar, P. *et al.* Mutations in the Na^+/K^+ -ATPase α_3 gene ATP1A3 are associated with rapid-onset dystonia parkinsonism. *Neuron* **43,** 169–175 (2004).
27. Cornelius, F., Turner, N. & Christensen, H. R. Modulation of Na,K-ATPase by phospholipids and cholesterol. II. Steady-state and presteady-state kinetics. *Biochemistry* **42,** 8541–8549 (2003).
28. Sotomayor, C. P., Aguilar, L. F., Cuevas, F. J., Helms, M. K. & Jameson, D. M. Modulation of pig kidney Na^+/K^+-ATPase activity by cholesterol: role of hydration. *Biochemistry* **39,** 10928–10935 (2000).
29. Colonna, T. E., Huynh, L. & Fambrough, D. M. Subunit interactions in the Na,K-ATPase explored with the yeast two-hybrid system. *J. Biol. Chem.* **272,** 12366–12372 (1997).
30. Toyoshima, C. *et al.* Modeling of the inhibitory interaction of phospholamban with the Ca^{2+} ATPase. *Proc. Natl Acad. Sci. USA* **100,** 467–472 (2003).

Supplementary Information is linked to the online version of the paper at www.nature.com/nature.

Acknowledgements We thank M. Kawamoto and N. Shimizu for their help in data collection at BL41XU, SPring-8, and T. Tsuda for many aspects of this work. We are grateful to D. B. McIntosh for his help in improving the manuscript and H. R.Z. Christensen for technical assistance. Thanks are also due to G. Cramb for sharing sequencing results of the β-subunit with us before publication. This work was supported by a Specially Promoted Project Grant from the Ministry of Education, Culture, Sports, Science and Technology of Japan, to C.T., and grants from the Danish Medical Research Council, to F.C.

Author Information Atomic coordinates and structure factors for the structure reported in this work have been deposited in the Protein Data Bank under accession number 2ZXE. Reprints and permissions information is available at www.nature.com/reprints. Correspondence and requests for materials should be addressed to C.T. (ct@iam.u-tokyo.ac.jp).

METHODS

Preparation of shark Na^+, K^+-ATPase. Crude membrane fractions (microsomes) from the rectal gland of the shark *Squalus acanthias* were prepared by homogenization followed by washing and isolation by centrifugation in 30 mM histidine, 1 mM EDTA, 0.25 M sucrose, pH 6.8. The microsomal preparation was subsequently purified by sucrose flotation[31]. The microsomes were diluted to 40% sucrose and layered on top of 60% sucrose followed by layers of 35% sucrose and histidine/EDTA buffer without sucrose. After centrifugation at 96,000*g* for 2 h at 4 °C, the bands at the 0/35% and 35/40% interfaces were collected, washed and resuspended in the histidine/EDTA buffer with 0.25 M sucrose.

The purified microsomes were washed with ~0.15% deoxycholate to remove extrinsic proteins and to open sealed vesicles. Then a purified membrane preparation was obtained by differential centrifugation essentially as described previously[32]. The preparation was suspended in the histidine/EDTA buffer with 25% glycerol and kept at −20 or −80 °C until use. The preparation showed a turnover number of 200 s^{-1} at 37 °C.

Crystallization. Solubilised ATPase with octaethyleneglycol mono-*n*-dodecylether ($C_{12}E_8$) was mixed with a buffer supplemented with exogenous phosphatidylcholine, consisting of 100 mM KCl, 4 mM $MgCl_2$, 8 mM KF, 5 mM glutathione, 15 mg ml^{-1} $C_{12}E_8$, 20% (w/v) glycerol and 20 mM Tris buffer/HCl, pH 7.0, so that the final concentrations of ATPase and phosphatidylcholine were 2.5 mg ml^{-1} and 2.1 mg ml^{-1}, respectively. The solution was put in dialysis buttons and dialysed against a buffer consisting of 18% (w/v) polyethyleneglycol 3000, 25% glycerol (w/v), 5% (v/v) 2-methyl-2,4-pentanediol, 100 mM potassium acetate, 10 mM KCl, 4 mM $MgCl_2$, 4 mM KF, 0.1 mM EGTA, 10 mM glutathione, 2 μg ml^{-1} 2,6-di-*t*-butyl-*p*-cresol, 20 mM MES/Tris buffer, pH 7.0, at 25 °C for 1–2 months. Before flash freezing with cold nitrogen gas, the specimen was dialysed overnight against the same buffer but containing 40% (w/v) polyethyleneglycol 3000. This treatment shrank the *a*-axis dimension and improved the resolution.

Structure determination and analysis. All the diffraction data were collected at BL41XU of SPring-8, Japan, at 100 K using ADSC Q315 and Rayonix E255HE charge-coupled-device detectors. The wavelength used was 0.9 Å for the native data sets and those corresponding to respective absorption peaks for the derivatives. DENZO and SCALEPACK[33] were used to process diffraction data. The crystals belonged to the *C*2 space group with unit-cell parameters of $a = 223.8$ Å, $b = 50.9$ Å, $c = 163.8$ Å and $\beta = 105.1°$. The *a*-axis dimension varied between 219 and 226 Å. MLPHARE in the CCP4 package[34] was used for MIRAS (multiple isomorphous replacement with anomalous scattering) phasing. The mean figure of merit was 0.55 using MIRAS and 0.98 after density modification with CNS[35]. Molecular replacement and refinement were carried out with CNS, and finally with REFMAC[36]. Fractions of residues (1,134 altogether, excluding Gly and Pro) in the most favoured, additionally allowed, generously allowed and disallowed regions of the Ramachandran plot are 84.0%, 14.9%, 1.2% and 0.0%, respectively, according to PROCHECK[37]. Hydrogen bonds were identified with HBPLUS[38]. Structural figures were prepared with TURBOFRODO (http://www.afmb.univ-mrs.fr/-TURBO-), MOLSCRIPT[39] and RASTER3D[40].

31. Jones, L. R. Rapid preparation of canine cardiac sarcolemmal vesicles by sucrose flotation. *Methods Enzymol.* **157,** 85–91 (1988).
32. Skou, J. C. & Esmann, M. Preparation of membrane Na^+,K^+-ATPase from rectal glands of *Squalus acanthias*. *Methods Enzymol.* **156,** 43–46 (1988).
33. Otwinowski, Z. & Minor, W. Processing of X-ray diffraction data collected in oscillation mode. *Methods Enzymol.* **276,** 307–326 (1997).
34. Collaborative Computational Project, Number 4. The CCP4 suite: programs for protein crystallography. *Acta Crystallogr. D* **50,** 760–763 (1994).
35. Brünger, A. T. *et al.* Crystallography & NMR system: A new software suite for macromolecular structure determination. *Acta Crystallogr. D* **54,** 905–921 (1998).
36. Murshudov, G. N., Vagin, A. A., Lebedev, A., Wilson, K. S. & Dodson, E. J. Efficient anisotropic refinement of macromolecular structures using FFT. *Acta Crystallogr. D* **55,** 247–255 (1999).
37. Laskowski, R. A., Moss, D. S. & Thornton, J. M. Main-chain bond lengths and bond angles in protein structures. *J. Mol. Biol.* **231,** 1049–1067 (1993).
38. McDonald, I. K. & Thornton, J. M. Satisfying hydrogen bonding potential in proteins. *J. Mol. Biol.* **238,** 777–793 (1994).
39. Kraulis, P. J. MOLSCRIPT: a program to produce both detailed and schematic plots of protein structures. *J. Appl. Crystallogr.* **24,** 946–950 (1991).
40. Merritt, E. A. & Bacon, D. J. Raster3D: Photorealistic molecular graphics. *Methods Enzymol.* **277,** 505–524 (1997).